Citation:
Ke, X.; Duan, Y., A spatially-varying relaxation parameter Lattice Boltzmann Method (SVRP-LBM) for predicting the effective thermal conductivity of composite material. 2019, 169, 109080.
https://doi.org/10.1016/j.commatsci.2019.109080

A spatially-varying relaxation parameter Lattice Boltzmann Method (SVRP-LBM) for predicting the effective thermal conductivity of composite material

Xinyuan Ke[1]* Yu Duan[2]

1. Department of Architecture and Civil Engineering, University of Bath, Bath BA2 7AY, United Kingdom
2. Department of Mechanical Engineering, Imperial College London, London, UK

*Corresponding author. E-mail: x.ke@bath.ac.uk, Tel: +44 (0) 1225 384020

Highlights

- An in-house coded SVRT-LBM solver for predicting effective thermal conductivity
- An optimized method to choose spatially varying relaxation parameters
- Taking into consideration contact resistance, filler geometry and size distribution

Graphic abstract

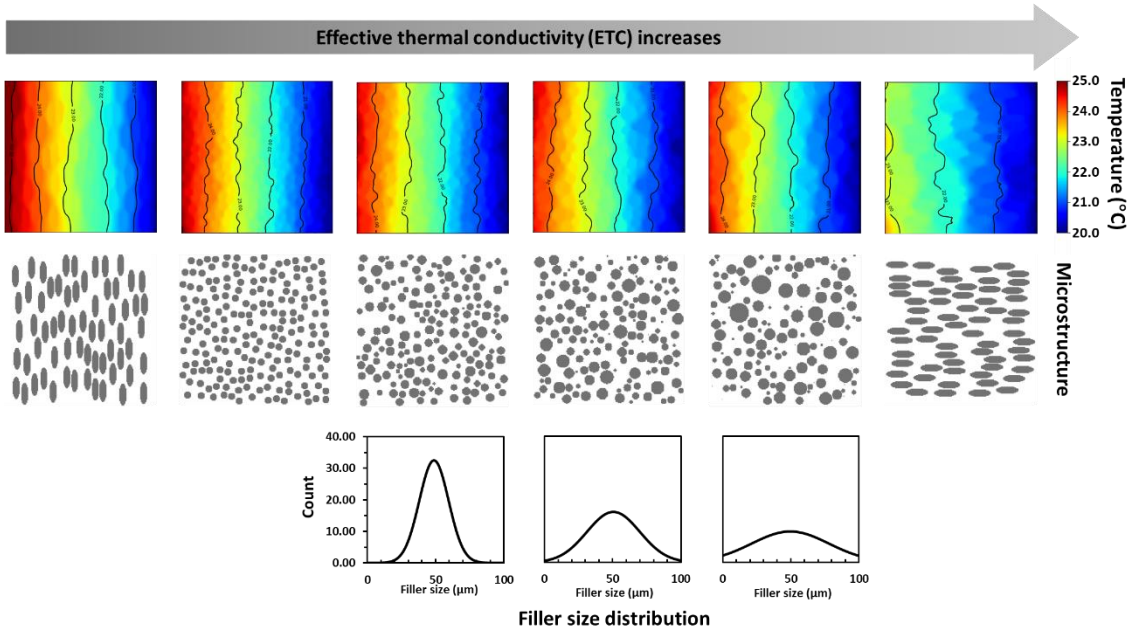

A SVRP-LBM solver for predicting the effective thermal conductivities of composite materials with varying fillers size distributions and geometries.

Abstract

Citation:
Ke, X.; Duan, Y., A spatially-varying relaxation parameter Lattice Boltzmann Method (SVRP-LBM) for predicting the effective thermal conductivity of composite material. 2019, 169, 109080.
https://doi.org/10.1016/j.commatsci.2019.109080

Functional filler-reinforced composite materials play critical roles in thermal management in various engineering applications. In this study, an in-house coded spatially-varying relaxation parameter Lattice Boltzmann Method (SVRP-LBM) solver has been developed for predicting the effective thermal conductivity (ETC) of simulated composite materials. A randomly dispersed filler generator (RDFG) incorporating Monte Carlo random sampling method has been developed for reconstructing the microstructure of composite materials. The artificial composite materials with functional fillers of different geometries and particle size are studied. The SVRP-LBM is validated against FVM perditions and theoretical models. The spatially-varying relaxation parameters method has been used to reflect materials with different thermophysical properties, including the interfacial contact resistance between the matrix-filler interfaces. It is demonstrated that the lowest relaxation parameters should be around 1.0 in order to achieve a higher accuracy of LBM predictions. The effects of filler geometry and particle sizes on the ETC are also assessed. The shape and orientation of the anisotropic filler have strong effects on the ETC. After the geometry of the filler in the numerical models being adjusted accordingly to the real fillers, the predictions show good agreement with experimental data. All in all, the SVRP-LBM solver has shown good capability and accuracy for predicting the ETC of composite material.

Keywords:

Lattice Boltzmann
Spatially-varying relaxation parameters
Numerical prediction
Composite materials
Effective thermal conductivity

Citation:
Ke, X.; Duan, Y., A spatially-varying relaxation parameter Lattice Boltzmann Method (SVRP-LBM) for predicting the effective thermal conductivity of composite material. 2019, 169, 109080.
https://doi.org/10.1016/j.commatsci.2019.109080

58 ## Nomenclature

Letters

c_s	Pseudo sound speed (m/s)
$\vec{c}_i$	Discrete lattice speed at direction *i* (m/s)
d	Dimensionless LBM diffusion coefficient
f_i	Distribution function
f_i^{eq}	Equilibrium distribution function
i	D2Q9 LBM velocity direction (i=0~8)
k	Thermal conductivity (W/m·K)
k_{eff}	Effective thermal conductivity (W/m·K)
q	Heat flux (W/m^2)
$\vec{r}$	Position vector (m)
t	Time (s)
t_{LBM}	Dimensionless LBM time step
w_i	Weighting factor at direction *i*
A	Composite cross-sectional area (m^2)
C_p	Specific thermal capacity (J/kg·K)
D_{diff}	Thermal diffusivity (m^2/s)
L	Composite thickness (m)
N	Total number of lattice
T	Temperature (K)
ΔT	Temperature difference (K)

Greek symbols

ρ	Density (kg/m^3)
τ	Dimensionless relaxation time
ξ	Average particle size (mean value)
σ^2	Variance
φ	Filler volume fraction
φ_n	Volume fraction of phase n (n=1, 2, 3 …)
ω	Dimensionless relaxation parameter
Ω_i	Collision operator at direction *i*

59

60

61

Citation:
Ke, X.; Duan, Y., A spatially-varying relaxation parameter Lattice Boltzmann Method (SVRP-LBM) for predicting the effective thermal conductivity of composite material. 2019, 169, 109080.
https://doi.org/10.1016/j.commatsci.2019.109080

1 Introduction

In recent decades, there has been rapid progress in the synthesis and processing of composite materials enhanced with functional fillers [1-3]. These functional filler-reinforced composite materials are widely used for thermal management in various applications, such as energy storage [4], electrolyte fuel cell [5], small electronic devices [6, 7], and thermal insulation in buildings [8]. As these materials play more and more important roles in our everyday life, there have been increasing demands for better scientific understanding of the heat transfer process within these materials at microscopic and mesoscopic scales [9].

Thermal conduction is the main heat transfer mechanism that occurs in composite materials [10, 11]. The thermal conductivity of composite material plays critical roles in assessing its thermal performances, such as thermal insulation and heat dissipation [11-13]. The effective thermal conductivity (ETC) is the most commonly used parameter for characterising the thermal performance of composite materials [11, 14]. The ETC of a composite material is determined by many factors, including the thermophysical properties of both the matrix and filler materials, volume fractions, geometries and distributions of the functional fillers [10, 13, 15]. Both experimental methods and modelling methods can be used to assess the ETC values. The experimental methods include steady-state methods, such as guarded hot plate method, axial flow method, and heat flow meter method; and transient methods, such as flash method, transient hot-wire method, and transient plane source method [16]. The modelling methods include theoretical modelling and numerical modelling. The theoretical models for composite materials can be categorized into two classes, the effective medium approximation (EMA) and the micromechanics method. The EMA methods include the Maxwell-Eucken model [17] and its extensions, while the micromechanics method includes Mori–Tanaka (M-T) model [18] and Benvensite's model [17]. A summary of these existing theoretical models for predicting ETC of polymer-based composite material can be found in Zhai et al. [14].

Owing to the recent development of computational techniques, numerical simulation methods have attracted growing attention as powerful tools to predict the ETC of composite materials at multiple scales [14]. The finite-difference methods (FDM) and finite volume method (FVM) are widely used for the macroscale (>1mm) thermal performance modelling [19, 20]. In comparison, the Lattice Boltzmann Method (LBM) shows better precision and faster time evolution when dealing with heat transfer at mesoscales (1μm to 1mm) [21-23]. However, when the nanomaterials (1nm to 1μm) are used as functional fillers, such as 2D graphene sheets, molecular dynamic (MD) models are often used to reconstruct their nanoscale features [24]. For functional composite materials, the scales of the fillers, such as metals [1, 25], functional ceramics [6, 7], and graphite [2, 26], are normally around few micrometres, making the LBM a better method to simulate the thermal performance of these materials.

Citation:
Ke, X.; Duan, Y., A spatially-varying relaxation parameter Lattice Boltzmann Method (SVRP-LBM) for predicting the effective thermal conductivity of composite material. 2019, 169, 109080.
https://doi.org/10.1016/j.commatsci.2019.109080

The Lattice Boltzmann Method (LBM), originated from the lattice gas automata (LGA) method and developed based on the Boltzmann kinetic equation is a powerful mesoscopic approach. The method can cooperate with the complex geometry boundary conditions and various interactions between particles [14, 21]. Wang et al. [27] used LBM to predict the ETC of a random open foam porous material. Lu et al. [28] studied the conjugate heat transfer phenomena at the solid-liquid interfaces using LBM. Fang et al. [29] used LBM to predict the thermal conductivity of braided fabric composites. And, Li et al. [7] used the same method to study the effects of fillers size on the ETC of thermal interfacial material for the heat dissipation in LED.

Despite the recent progress in using LBM to predict the ETC of composite materials, tuning of relaxation parameters in order to achieve stable and accurate simulations remains as a challenge [30]. In general, the choice of suitable relaxation parameter (ω) is crucial for the accuracy and stableness of the LBM simulation [23, 30]. Wang et al. [31] suggested that the ω should be between 0.5 to 2 to ensure stableness for the simulation of the conjugate heat transfer at the solid-liquid interfaces. Walther et al. [23] suggested that for the ionic diffusion process in two-phase materials with large diffusivity ratios, stable LBM simulation results can only be achieved when the ω for both materials is within 0.1 and 1.0. However, the effect of ω values on simulation accuracy has not yet been discussed.

The Monte Carlo random sampling method has been applied for generating of microstructures which is representative of laboratory synthesised materials [22, 32]. Zhou et al. [22] used randomly dispersed fillers with uniformly distributed filler sizes. This treatment has its limitation to represent the actual microstructure of composite materials, as particle distributions similar to the normal distribution were often observed in experiments [6]. Deng et al. [33] used statistical self-similarity fractal geometry to reconstruct the self-similar random porous structure; however, the fixed filler location was adapted which was not ideal to represent the composite materials reinforced by randomly dispersed fillers. It remains unclear how the distribution of particle sizes will affect the thermal performance of a composite. The shape of the particles impacts the macroscale thermal properties of the composite material, and should not be neglected [10]. Moreover, the effects of the orientation of fillers need to be better understood, if the filler particles possess the anisotropic shape. In addition, the heat conduction occurred at the interfaces between the functional filler and the matrix material also plays critical roles in the overall thermal performance of the composite material [34-36]. The main physical phenomenon to consider here is interfacial contact resistance due to imperfect contact (or roughness) between the surfaces that leads to large phonon scattering and temperature differences [37]. It would be necessary to test the ability of the LBM solver to reflect this physical phenomenon.

In this study, an in-house coded spatially-varying relaxation parameter Lattice Boltzmann Method (SVRP-LBM) solver has been developed for predicting the ETC of various composite materials. The paper is organised as follows: a brief introduction

Citation:
Ke, X.; Duan, Y., A spatially-varying relaxation parameter Lattice Boltzmann Method (SVRP-LBM) for predicting the effective thermal conductivity of composite material. 2019, 169, 109080.
https://doi.org/10.1016/j.commatsci.2019.109080

to the LBM method and randomly dispersed filler generator are included in section 2. Section 3 is contributed to discuss the benchmark study as well as the effect of the spatially varying relaxation parameters on the stableness and accuracy of the LBM simulation. In section 4, the effect of the random features of the fillers, distribution of filler size and location and orientation of the anisotropic fillers, the thermal conduction behaviours between the filler and matrix interfaces are discussed, as well as validation of the SVRP-LBM solver with respect to the real composite materials.

2 Methodologies

2.1 Governing equations

The heat conduction in the lattice domain is governed by equation (1),

$$\rho C_p \frac{\partial T}{\partial t} = k\nabla^2 T \quad (1)$$

where ρ, C_p and k are the density, specific thermal capacity, and thermal conductivity of the material, respectively.

2.2. Lattice Boltzmann method

In this paper, the single-relaxation-time D2Q9 LBM is used. We will give a brief introduction to the methodology in this section. For readers' interested in this method, please refer to [30, 38] for more information.

The kinetic LB equation can be written as,

$$\frac{\partial f_i(\vec{r},t)}{\partial t} + \vec{c}_i \cdot \frac{\partial f_i(\vec{r},t)}{\partial \vec{r}} = \Omega_i \quad (2)$$

where $f_i(\vec{r},t)$ represents the probability distribution function in direction i (i=0~8, Figure 1) at location $\vec{r}$ at time t. Ω_i is the collision operator.

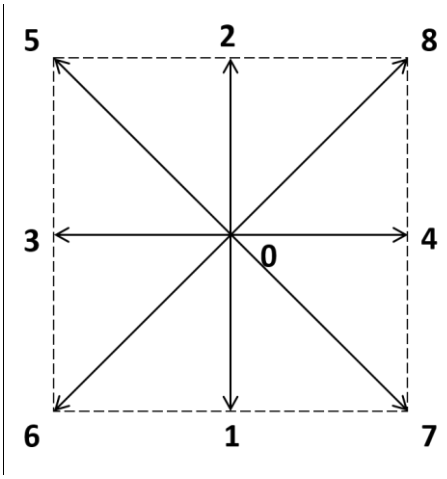

Figure 1 Schematic diagram of D2Q9 velocity directions model.

Citation:
Ke, X.; Duan, Y., A spatially-varying relaxation parameter Lattice Boltzmann Method (SVRP-LBM) for predicting the effective thermal conductivity of composite material. 2019, 169, 109080.
https://doi.org/10.1016/j.commatsci.2019.109080

168

169 In this study, the Bhatnagar-Gross-Krook (BGK) collision approximation is used,
170 which can be written as [39],

$$\Omega_i = -\frac{1}{\tau}[f_i(\vec{r},t) - f_i^{eq}(\vec{r},t)] \quad (3)$$

$$\Delta\vec{r} = \Delta t \cdot \vec{c}_i \quad (4)$$

171 where f_i^{eq} is the equilibrium distribution function and τ is the relaxation time. $\vec{c}_i$ is
172 the lattice speed at direction *i*.

173 The discretization of equation (2) to (4) can be written as following,

$$f_i(\vec{r} + \Delta t \cdot \vec{c}_i,\ t + \Delta t) - f_i(\vec{r},t) = -\omega \cdot [f_i(\vec{r},t) - f_i^{eq}(\vec{r},t)] \quad (5)$$

$$\omega = \frac{\Delta t}{\tau} \quad (6)$$

174 where ω is the relaxation parameter.

175 The bulk properties of density and temperature are obtained by equation (7),

$$T(\vec{r},\ t) = \sum_0^8 f_i(\vec{r},\ t) \quad (7)$$

176 where *T* represents the macroscopic temperature.

177 The macroscopic temperature distribution correlates with the mesoscopic
178 equilibrium distribution function via equation (8) and (9),

$$f_i^{eq} = w_i \cdot T(\vec{r},t) \quad (8)$$

$$w_i := \begin{cases} \frac{4}{9} & i = 0 \\ \frac{1}{9} & i = 1\sim4 \\ \frac{1}{36} & i = 5\sim8 \end{cases} \quad (9)$$

179 where w_i is the weighting factor for direction *i* (Figure 1).

180 The discrete lattice velocity $\vec{c}_i$ is defined as,

$$\vec{c}_i := \begin{cases} 0 \quad i = 0 \\ (cos\theta_i, sin\theta_i) \cdot c_s, \quad \theta_i = (i-1)\frac{\pi}{2} \quad i = 1\sim4 \\ \sqrt{2}(cos\theta_i, sin\theta_i) \cdot c_s, \quad \theta_i = (i-5)\frac{\pi}{2} + \frac{\pi}{4} \quad i = 5\sim8 \end{cases} \quad (10)$$

181 where c_s is the pseudo sound speed.

182 According to the Chapman-Enskog Expansion [38], the relaxation parameter ω is
183 related to the thermal conductivity and thermal diffusivity (D_{diff}) of the material via
184 equations (11) and (12),

Citation:
Ke, X.; Duan, Y., A spatially-varying relaxation parameter Lattice Boltzmann Method (SVRP-LBM) for predicting the effective thermal conductivity of composite material. 2019, 169, 109080.
https://doi.org/10.1016/j.commatsci.2019.109080

$$\frac{k}{\rho C_p} = \frac{{c_s}^2 \cdot \Delta t}{2}\left(\frac{1}{\omega} - \frac{1}{2}\right) \tag{11}$$

$$D_{diff} = \frac{k}{\rho C_p} \tag{12}$$

where $0<\omega<2$.

In this study, spatially varying relaxation parameters (SVRP) are used to reflect the heterogeneous thermophysical properties of composite materials at mesoscale [31]. For composite materials composed of two materials, their thermophysical properties are related to the relaxation parameters as:

$$\frac{D_1}{D_2} = \frac{k_1}{k_2} \times \frac{(\rho C_p)_2}{(\rho C_p)_1} = \frac{\left(\frac{1}{\omega_1} - \frac{1}{2}\right)}{\left(\frac{1}{\omega_2} - \frac{1}{2}\right)} \tag{13}$$

After the system reaches its equilibrium final state, the effective thermal conductivity (ETC) is then calculated using equation (14),

$$k_{eff} = \frac{L \cdot \int q \cdot dA}{\Delta T \cdot \int dA} \tag{14}$$

where q is the steady state heat flux, ΔT is the temperature difference along the heat flux direction over a distance of L, and A is the cross-sectional area.

2.2 Boundary conditions

The insulated boundaries are treated as adiabatic. The isothermal boundary condition follows the Zou and He bounce-back rule [40], which can be expressed as:

$$f_\alpha - f_\alpha^{eq} = -(f_\beta - f_\beta^{eq}) \tag{15}$$

where α and β represent the two opposite directions.

Equation (16) is used to approximate the heat flux at the constant heat flux boundary condition.

$$q' = -k_{phase} \cdot \frac{\partial T}{\partial \vec{r}} \tag{16}$$

2.3 Randomly dispersed filler generator (RDFG)

In this study, a randomly dispersed filler generator (RDFG) has been developed to mimic microstructures of artificial composite materials. In the RDFG, the scale of the fillers are governed by the normal distribution $f(x|\mu,\sigma^2)$, which expressed by equation (17). Meanwhile, the location of the fillers in the domain follows the uniform distribution. Overlapping of the located fillers is not allowed in this practice. The contact between the fillers (sharing of the same node) is only allowed when the total filler fraction is higher than 0.3.

Citation:
Ke, X.; Duan, Y., A spatially-varying relaxation parameter Lattice Boltzmann Method (SVRP-LBM) for predicting the effective thermal conductivity of composite material. 2019, 169, 109080.
https://doi.org/10.1016/j.commatsci.2019.109080

$$f(x|\xi,\sigma^2)=\frac{1}{\sqrt{2\pi\sigma^2}}e^{-\frac{(x-\xi)^2}{2\sigma^2}} \quad (17)$$

where ξ is the average particle size and σ^2 is the variance,

For the RDFG developed in this study, the average particle size and variance are provided by the users as initial inputs, as well as the total filler volume fraction. For any given number of total fillers, the scalers following the normal distribution as shown in equation (17) will be generated, randomly allocated to the lattice domain and output as black (filler) and white (matrix) images. The total filler volume fraction will be calculated by counting the percentage of black pixels in the entire lattice domain. To achieve a designated total volume fraction, an initial filler number is estimated using the average particle size provided by the user, which will be adjusted stepwise until reaching the designated total filler volume. Since the least increment/decrement possible is depending on the smallest fillers generated following the normal distribution, a deviation below 1.0 % is considered acceptable by the RDFG.

Figure 2 gives a view of four simulated artificial composite materials microstructure generated using RDFG with different input parameters, according to the scanning electron microscopy (SEM), or transmission electron microscopy (TEM) images reported in the literature [41-44]. Figure 3 and Figure 4 show examples of simulated microstructure of composite material consist of fillers (spherical or elliptical) with varying sizes. And, sizes of the particles in each composite follow the normal distribution.

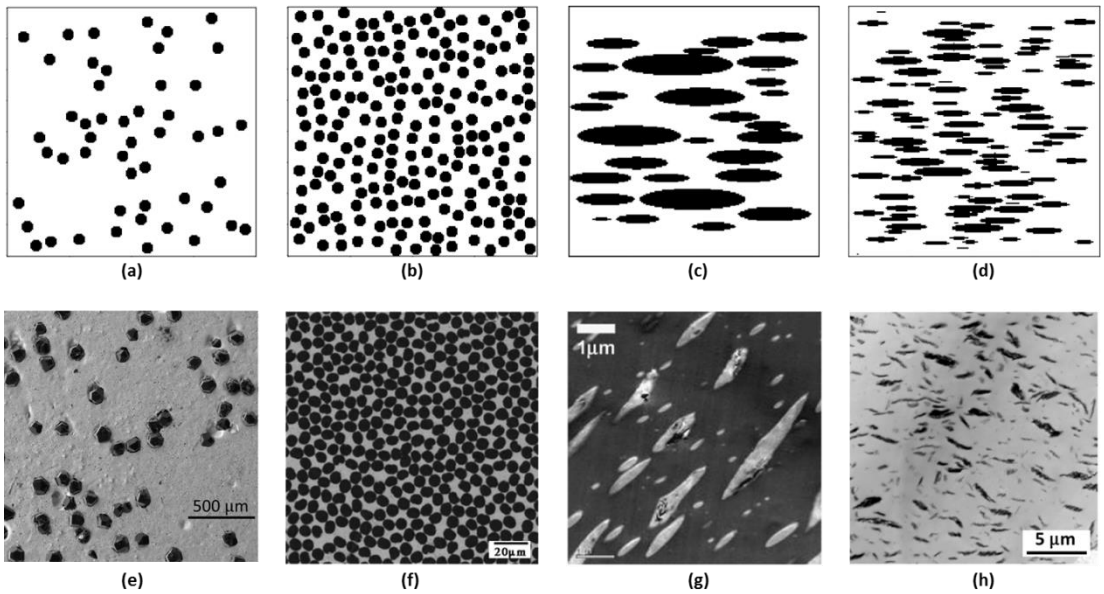

Figure 2 (a) to (d), schematics of the generated composite material microstructure with fillers of different sizes, geometries and volume fractions using the described

RDFG computational method (200x200), and comparison with the microstructure of real composite materials. (e) SEM image of Cu/D composite, adapted from [41] with permission from Elsevier; (f) BSE image of carbon fibre reinforced bulk metallic glass composite, reproduced from [42], with the permission of AIP Publishing; (g) TEM image of a typical PC/PBT/Talc composite, adapted from [43] with permission from Elsevier; (h) TEM image of PLA/talc composite, adapted from [44] with permission from John Wiley and Sons;

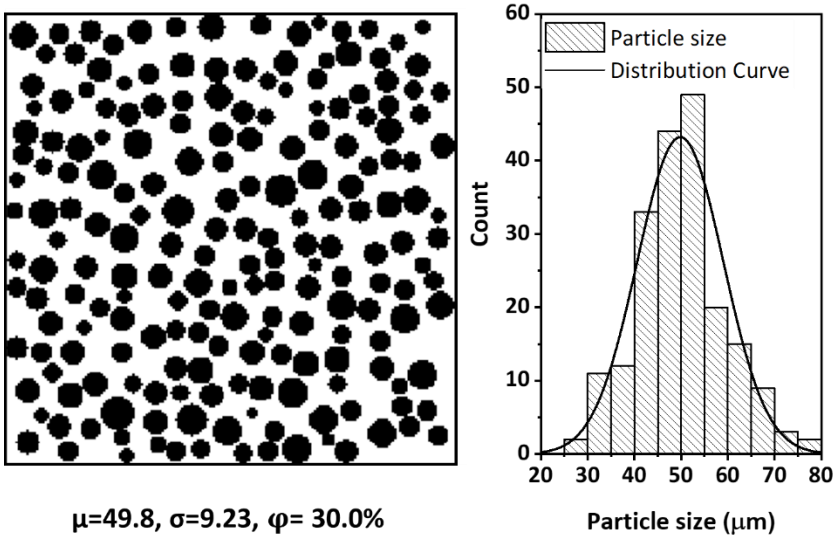

Figure 3 Schematic diagram of the microstructure with spherical fillers of normally distributed particle sizes.

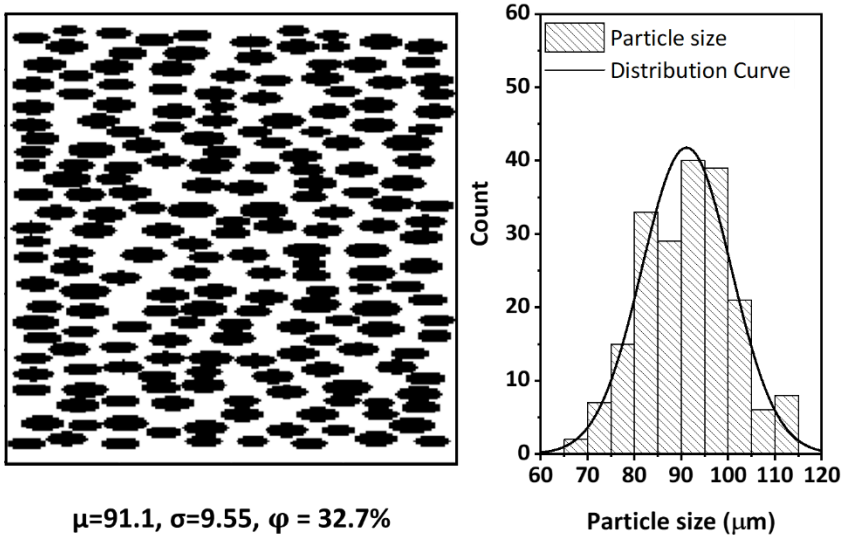

Figure 4 Schematic diagram of the microstructure with elliptical fillers of normally distributed particle sizes. The values of semi-major axis of the ellipses were used for plotting the particle size distribution.

Citation:
Ke, X.; Duan, Y., A spatially-varying relaxation parameter Lattice Boltzmann Method (SVRP-LBM) for predicting the effective thermal conductivity of composite material. 2019, 169, 109080.
https://doi.org/10.1016/j.commatsci.2019.109080

3 Benchmark Studies

3.1 Comparison with the finite volume method

Before applying the in-house developed LBM in the further application, the code is first validated against a simulation based on the finite volume method (FVM) in this section. It is worth to mention that the LBM code and RDFG are developed using Python 3, while the FVM is a Fortran code. In the FVM code, the heat conduction equation is discretized using the 2^{nd} order central differencing scheme. Two codes are applied to simulate the heat conduction via a plate which is made from two materials, Material I and II. The geometry of the validation case is illustrated in Figure 5. Both materials possess different thermal conductivities and diffusivities. The dimensionless conductivity and diffusivity of Material I are k_1=1.0 and D_1=0.05, respectively, while these two properties (dimensionless) of Material II are k_2 =10.0, D_2 =0.25. The Material II occupies the bottom left quarter, while elsewhere is filled with Material I. The dimensionless temperature on the west and south wall are set as T=1, while the dimensionless temperature on the other two walls are set as T=0.

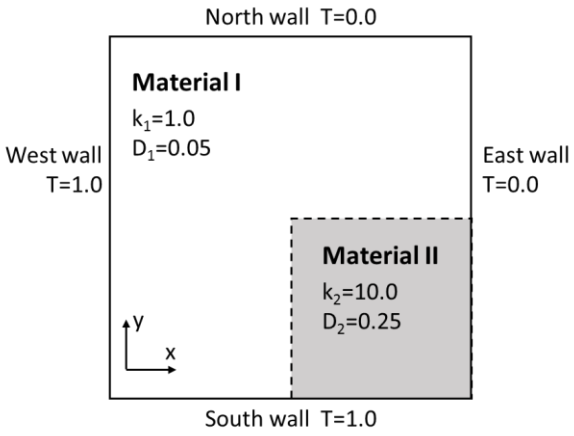

Figure 5 Schematic diagram of 2-D problem with dimensionless boundary conditions and thermophysical properties of different materials. The length along x-axis and y axis both have been set to 1(dimensionless).

For the LBM simulation, a lattice domain of 200×200 is used. The relaxation parameter ω_1 and ω_2 of material I and II are determined according to equation (13). The ω_1 and ω_2 in the current case are set as 1.67 and 1.00, respectively. In the FVM simulation, the domain is discretized using the 80×80 mesh. The mesh independent is achieved in the FVM simulation.

The temperature outputs at the equilibrium state of both LBM and FVM simulations are compared in Figure 6. The temperature contours (Figure 6a) of both simulations show good agreement between two methods. To exam the results with more details, the vertical temperature profile at x = 0.265 and x = 0.760 are compared in Figure 6b. At x = 0.265, where the line crosses only the region of Material I, the

Citation:
Ke, X.; Duan, Y., A spatially-varying relaxation parameter Lattice Boltzmann Method (SVRP-LBM) for predicting the effective thermal conductivity of composite material. 2019, 169, 109080.
https://doi.org/10.1016/j.commatsci.2019.109080

temperature profiles by both methods overlap with each other. At x = 0.760, where the line crosses Material I and Material II, there shows an observable difference between the outputs of two methods. However, differences only appear around the interfaces between two materials. This inconsistency lies in the fundamental difference of two methods in the treatment of heat transfer around the interfaces. In the FVM, the heat transfer around the interfaces of two materials is approximated using the information from the cells at both sides of the interface because of the numerical scheme. In the LBM, different relaxation parameters are assigned to the lattice nodes within different materials, and no special treatment at the interfaces is made. But such difference is deemed to be ignorable as suggested in [45].

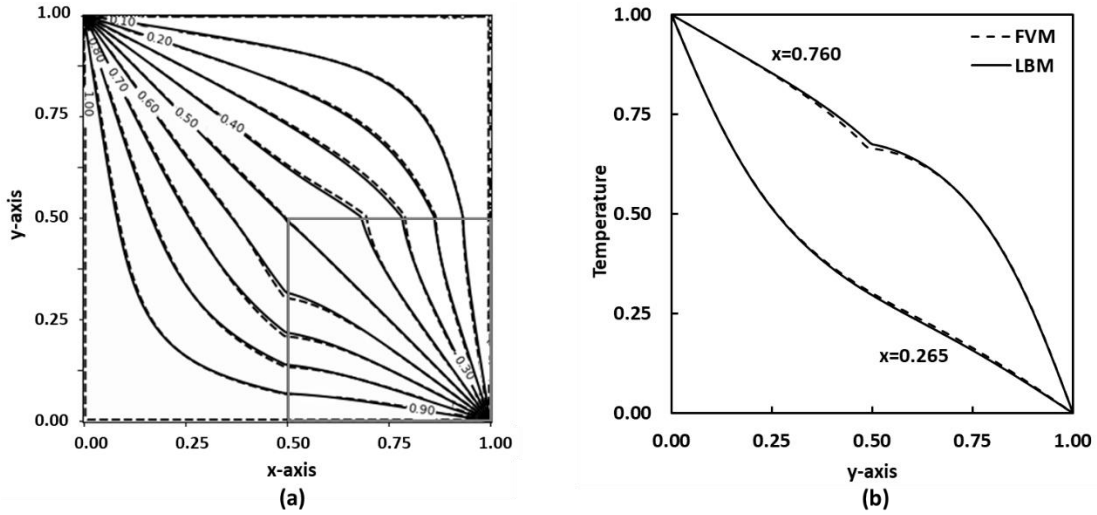

Figure 6 (a) Comparison between the LBM (solid lines) and FVM (dashed lines) prediction at the equilibrium steady state. (b) Comparison between the LBM (solid lines) and FVM (dashed lines) at x=0.265 and x=0.760.

3.2 Sensitivity study of relaxation parameters for high diffusivity ratios

In this section, the effects of the relaxation parameters on the accuracy and efficiency of the LBM simulation are discussed. As suggested by equation (13), the relaxation parameters ω_1 and ω_2 are related to the diffusivity ratio of two materials (D_1/D_2). Figure 7 shows the correlations between ω_1 and ω_2 when the D_1/D_2 ratio ranges from 0.001 to 1000. As illustrated in the figure, the values of ω_1 and ω_2 are positively correlated for a fixed D_1/D_2 ratio. When $0.01< D_1/D_2 <100$, it is easy to set one relaxation parameter to 1 while letting the other relaxation parameter to be slightly above 1 (over-relaxation). In the cases of large diffusivity ratios ($D_1/D_2 >$ 100 or $D_1/D_2 < 0.01$), one of the relaxation parameters has to be closer to the lower (0.0) or upper limit (2.0) of the allowed value, regardless of the other relaxation parameter, which might cause significant numerical instability [23].

Citation:
Ke, X.; Duan, Y., A spatially-varying relaxation parameter Lattice Boltzmann Method (SVRP-LBM) for predicting the effective thermal conductivity of composite material. 2019, 169, 109080.
https://doi.org/10.1016/j.commatsci.2019.109080

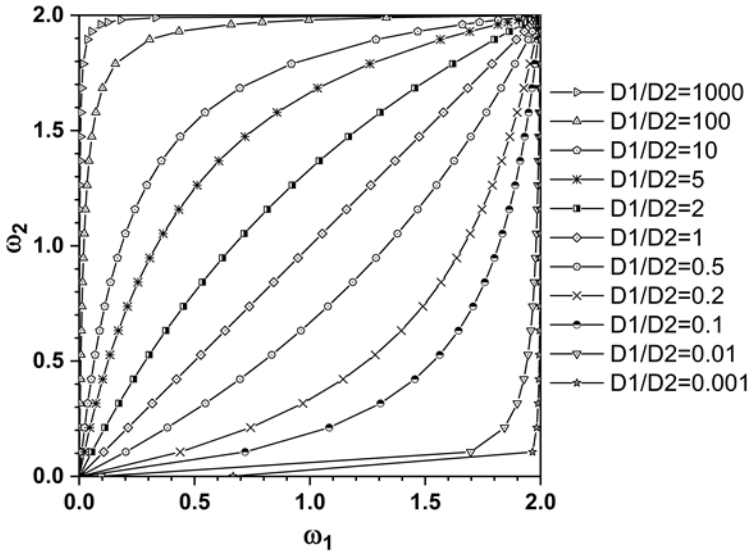

Figure 7 Relation between ω_1 and ω_2 when the diffusivity ratio D_1/D_2 ranges from 0.001 to 1000.

The LBM time step is related to the real-time scale via equation (18) and (19) [23, 38].

$$\frac{t}{t_{LBM}} = \frac{d \times L^2}{D \times N^2} \tag{18}$$

$$d = c_s^2 \left(\frac{1}{\omega} - \frac{1}{2}\right) \tag{19}$$

, where t, D and L represent the real-time, diffusion coefficient (m^2/s) and length scale, while t_{LBM}, d and N represent the dimensionless LBM time step, LBM diffusion coefficient and total number of lattice.

Figure 8 shows the correlations between the chosen relaxation parameters and the time evolution scale per LBM time step at the diffusivity ratio (D_1/D_2) of 100, whilst N is 200, L is 10^{-3} m, and D_2 is 1.0×10^{-6} m^2/s. As shown in the figure, the time evolution per LBM time step will always decrease as the selected relaxation parameter values increases, while the absolute value of the time evolution per iteration is dependent on the thermal property of the material and the resolution of the lattice.

Citation:
Ke, X.; Duan, Y., A spatially-varying relaxation parameter Lattice Boltzmann Method (SVRP-LBM) for predicting the effective thermal conductivity of composite material. 2019, 169, 109080.
https://doi.org/10.1016/j.commatsci.2019.109080

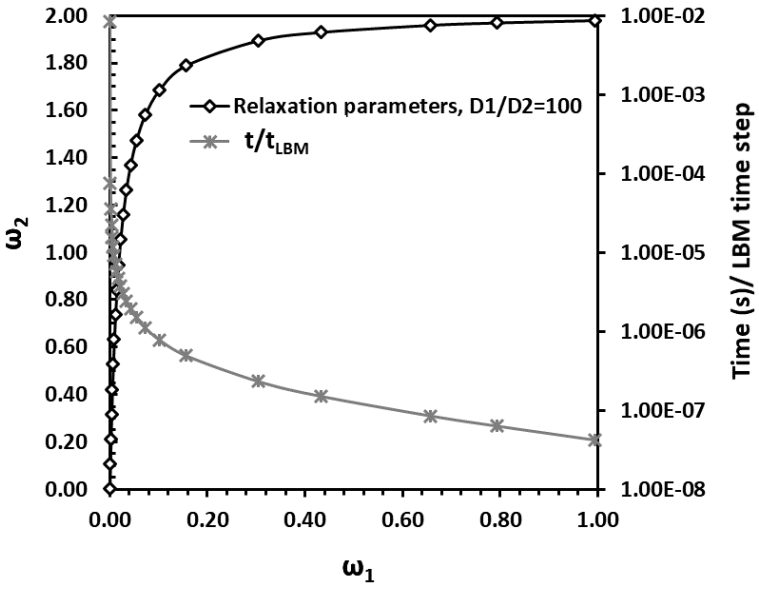

Figure 8 Relation between relaxation parameter ω_1 and ω_2 at the diffusivity ratio (D_1/D_2) of 100 (black line with diamond markers), and the time evolution per LBM time step (t/t_{LBM}) under the corresponded chosen relaxation parameter ω_1 and ω_2 (grey line with star markers).

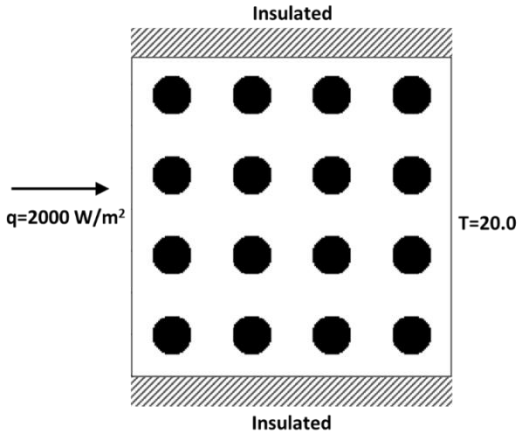

Figure 9 Schematic diagram of a periodically dispersed spheres model with boundary conditions

A case with periodically distributed spherical particles in the lattice domain is created to investigate the effect of the relaxation parameters on the simulation accuracy. A view of the geometry can be found in Figure 9. The conductivities of the spherical fillers and the main matrix are 1 W/m·K and 100 W/m·K, respectively. The heat flux on the left wall is set as 2000 W/m^2 and the temperature on the right wall is fixed at 20.0 °C while the other two walls are treated as adiabatic. The volume fraction of the fillers shown in Figure 9 is 20.6%.

Citation:
Ke, X.; Duan, Y., A spatially-varying relaxation parameter Lattice Boltzmann Method (SVRP-LBM) for predicting the effective thermal conductivity of composite material. 2019, 169, 109080.
https://doi.org/10.1016/j.commatsci.2019.109080

Figure 10 compares the predicted ETCs of the simulated composite using different relaxation parameters for these two materials. The least numbers of LBM time steps required for each case to reach the equilibrium final states are also plotted in Figure 10, together with the correlated real-time evolution based on the correlation shown in Figure 8. The predicted ETCs using different relaxation parameters are compared to the prediction using the Maxwell-Eucken model (equation (22)). More discussions about the Maxwell-Eucken model will be included in the next section. As the relaxation parameters increase, the accuracy of the LBM prediction (in comparison with theoretical values) increases, as well as the number of LBM time steps required for reaching the equilibrium state. The correlated real-time evolution at initial equilibrium decreased from 0.110s to 0.004s, as ω_1 increased from 0.005 to 0.660. However, after ω_1 being increased from 0.660 to 0.790, the ETC remains similar, while the total number of iteration required for reaching the equilibrium final state increases by approximately three times. The slight increase in the correlated time evolution when ω_1 is set to 0.79 is likely due to the nearly tripled LBM time steps required for the equilibrium state. The result here suggests that for a system with high diffusivity ratios, when the lower ω value approaches 1, the accuracy of the prediction increases as well as the LBM time steps required for the equilibrium state. In practical, a trade-off between prediction accuracy and simulation time needs to be considered.

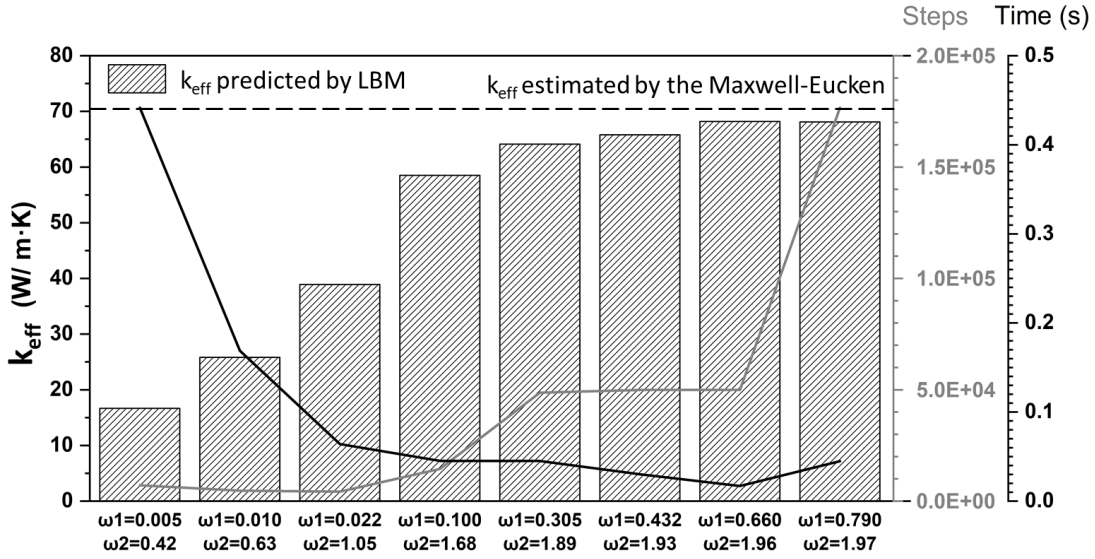

Figure 10 Evolution of calculated effective thermal conductivity (k_{eff}) versus LBM time steps, comparing the use of different relaxation times.

3.3 Comparison with Maxwell-Eucken model

The Maxwell-Eucken model, derived from the effective electric resistivity of a sphere containing N spherical particles based on the theory of electric potential satisfying the Laplace equation, is one of the most commonly used effective medium approximation (EMA) approach for predicting the ETCs of composites [46]. The Maxwell-Eucken model can be expressed as

Citation:
Ke, X.; Duan, Y., A spatially-varying relaxation parameter Lattice Boltzmann Method (SVRP-LBM) for predicting the effective thermal conductivity of composite material. 2019, 169, 109080.
https://doi.org/10.1016/j.commatsci.2019.109080

$$k_{eff} = k_1 \cdot \frac{2k_1 + k_2 + 2\varphi_2 \cdot (k_2 - k_1)}{2k_1 + k_2 - \varphi_2 \cdot (k_2 - k_1)} \quad (22)$$

, where k_1 and k_2 represent the thermal conductivities of the matrix and periodically dispersed spherical fillers, and $\varphi_2$represent the volume fraction of the filler.

The Maxwell-Eucken model is particularly effective for predicting the ETC of composite materials reinforced by low volume fraction well-dispersed particles. A view of the simulated case is included in Figure 9. The spherical fillers in the lattice domain distribute periodically and non-interacting. The volume heat capacity (ρC_p) of these artificial materials are set to be unity [21], which means $D_1/D_2 = k_1/k_2$. The thermal conductivity of the matrix is k_1 while the thermal conductivity of the filler is k_2. Under different k_1/k_2 ratios, k_1 is varying from 0.01 W/m·K to 100 W/m·K, while k_2 is fixed as 1 W/m·K. Hence, the D_1/D_2 ranges from 0.01 to 100. The relaxation parameters chosen for each material are selected according to the observations in section 3.2. More LBM time steps are required for reaching the equilibrium state when the k_1/k_2 becomes much larger (or smaller) than 1. Figure 11 compares the ETCs of artificial composites containing periodically dispersed spheres using LBM and Maxwell-Eucken model under different k_1/k_2 ratios. Well agreement between the theoretical Maxwell-Eucken model prediction and LBM prediction. The deviations between the predictions and the theoretical models are below 2.0%, the accuracy of which is sufficient enough for this application [27, 47]. This proves that the LBM algorithm developed in this study is valid for predicting the ETCs of composite materials reinforced by periodically dispersed spherical fillers under a wide range of k_1/k_2 values.

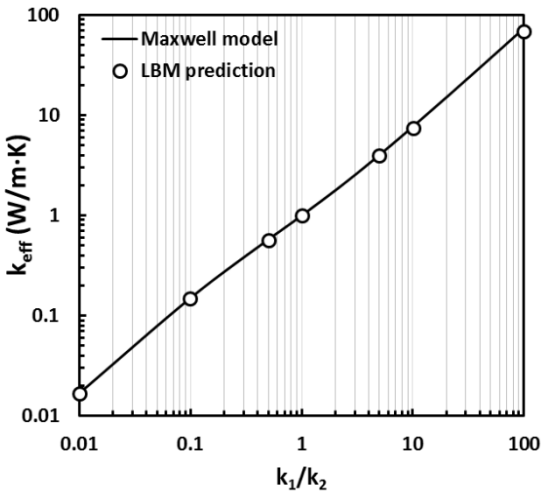

Figure 11 Predicted effective thermal conductivities of under different k_1/k_2.

Citation:
Ke, X.; Duan, Y., A spatially-varying relaxation parameter Lattice Boltzmann Method (SVRP-LBM) for predicting the effective thermal conductivity of composite material. 2019, 169, 109080.
https://doi.org/10.1016/j.commatsci.2019.109080

3.4 Comparison with serial and parallel models

Series and parallel models, with the interfaces of two materials either perpendicular or parallel to the heat flux direction (Figure 12a and c), are proposed to be used as the simplified representation of the complicated composite material microstructure [48]. The layers-in-series and the layers-in-parallel models are simplified representations of the highest and lowest estimated values in a two-phase composite material [1]. These two models also play very important roles in studying the interfacial effect between the two materials [28]. The theoretical models for predicting the ETCs of series and parallel models were derived based on circuit network of conductors [48], which can be expressed as equation (20) and (21), respectively.

$$k_{eff} = \frac{k_1 \cdot k_2}{\varphi_2 \cdot k_1 + \varphi_1 \cdot k_2} \tag{20}$$

$$k_{eff} = \varphi_1 \cdot k_1 + \varphi_2 \cdot k_2 \tag{21}$$

, in which φ_1 and φ_2 represent the volume fraction of materials with thermal conductivity of k_1 and k_2.

Again, ρC_p of these artificial materials are set to be unity [21], and the relaxation parameters for each material are selected as in the previous section. The k_2 value is kept at 1.0 while the k_1 value varies from 0.01 to 100. Figure 12 (b) and (d) compares the predicted ETCs using the LBM solver and the theoretical models. The results by the LBM solver show good agreement with theoretical values. The deviations between numerical outputs and theoretical values are within 1.0% for both series and parallel geometries. This again approves the good capability of this in-house LBM solver.

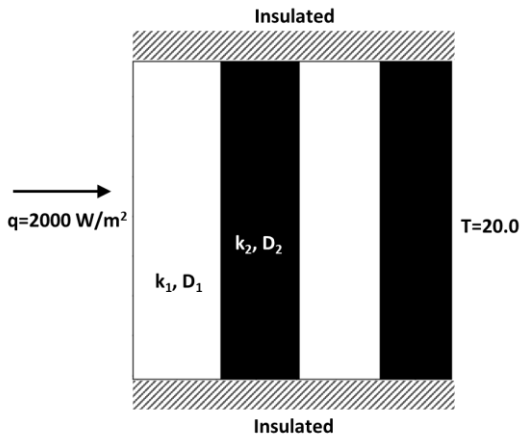

(a)

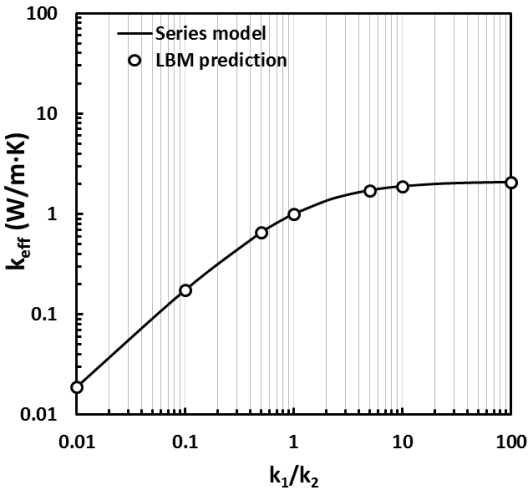

(b)

Citation:
Ke, X.; Duan, Y., A spatially-varying relaxation parameter Lattice Boltzmann Method (SVRP-LBM) for predicting the effective thermal conductivity of composite material. 2019, 169, 109080.
https://doi.org/10.1016/j.commatsci.2019.109080

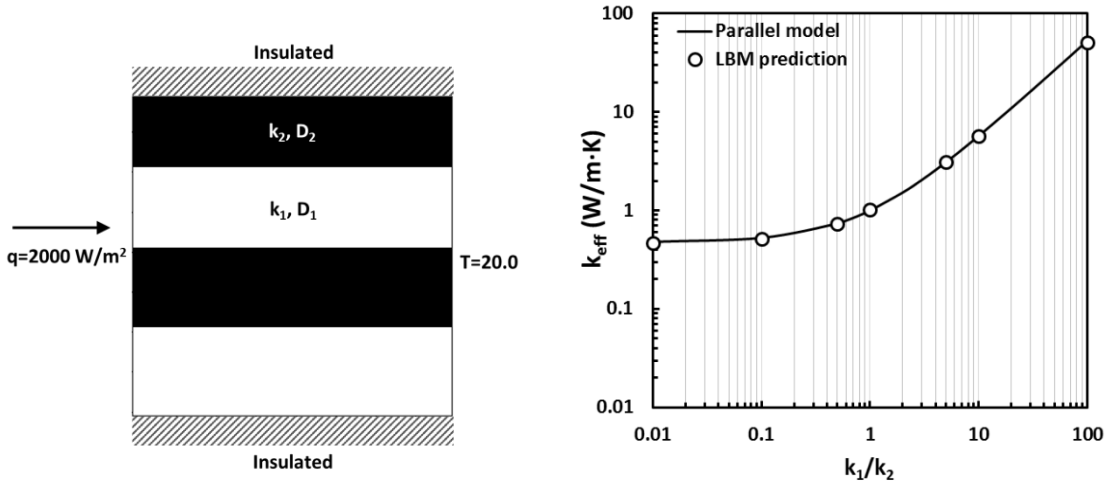

(c) (d)

Figure 12 Schematic diagram of (a) periodic series model , and (b) predicted effective thermal conductivities with different k_1/k_2 ratios; (c) periodic parallel model with boundary conditions, and (d) predicted effective thermal conductivities with different k_1/k_2 ratios. The k_2 value is kept as 1 W/m·K in all cases.

4 ETC of composite with randomly distributed fillers

4.1 Effect of shape and size of artificial representatives

The RDFG is used to generate the simulated composite materials reinforced by randomly dispersed fillers. Firstly, the effects of filler geometry (orientation and shape) on the thermal conduction of simulated composite materials are discussed (Figure 13 and Figure 14). Then the effects of filler size variation on the ETC are studied using spherical fillers following different size distribution (Figure 15).

To study the effects of orientations of anisotropic fillers, elliptical fillers with the aspect ratio of 3:1 and the minor axis value of 50 μm are generated, with their major axis either perpendicular (Figure 13A) or parallel to the heat flux direction (Figure 13C). These two orientations are chosen to represent the two extreme scenarios of the elliptical filler geometry in a composite material [49]. For studying the effect of filler shapes, spherical fillers of diameter 50 μm (Figure 13B) are generated as the comparison with the elliptical fillers. Spherical fillers of larger diameters, 70 μm (Figure 13D), are generated to studying the size effect. Three total filler volume fractions, 6.4%, 13.0% and 26.3%, are considered for each type of filler. In all of these cases, the thermal conductivity of the matrix materials is 0.2 W/m·K (k_1) and the thermal conductivity of the fillers (k_2) is 20.0 W/m·K. The volume heat capacities (ρC_p) of these artificial materials are set to be 1. The heat flux on the left wall (x=0) is 2000 W/m^2 and the temperature on the right wall (x = 1000 μm) is 20.0 °C while the other two walls (y=0 and y=1000 μm) are treated as adiabatic.

The temperature contour plots of these simulated composite materials (with total volume fraction of 26.3±0.4%) at the equilibrium states are shown in Figure 13. As expected, the temperature fields are influenced by the conductivities of the local

materials, and the non-uniform microstructure leads to the variation of temperature distribution perpendicular to the heat flux direction. According to the Fourier's law for heat conduction, the local temperature distribution within the sample matrix is positively correlated to the thermal conductivity of the material filled within the location. The local heat transfer would be more efficient (lower temperature gradient) within the highly thermal conductive filler materials than that within the matrix materials. This might explain the correlation between the filler geometry and the temperature distribution within the lattice domain as shown in Figure 13. Based on the temperature contours in the Figure 13, the highest temperature drop across the domain is observed in the case that the elliptical fillers are perpendicular to the heat flux direction (Figure 13A), while the lowest temperature gradient is observed from where the elliptical fillers are parallel to the heat flux direction (Figure 13C). In the case of spherical fillers, seeing Figure 13B and Figure 13D, a higher temperature gradient is shown in the lattice domain reinforced with smaller fillers.

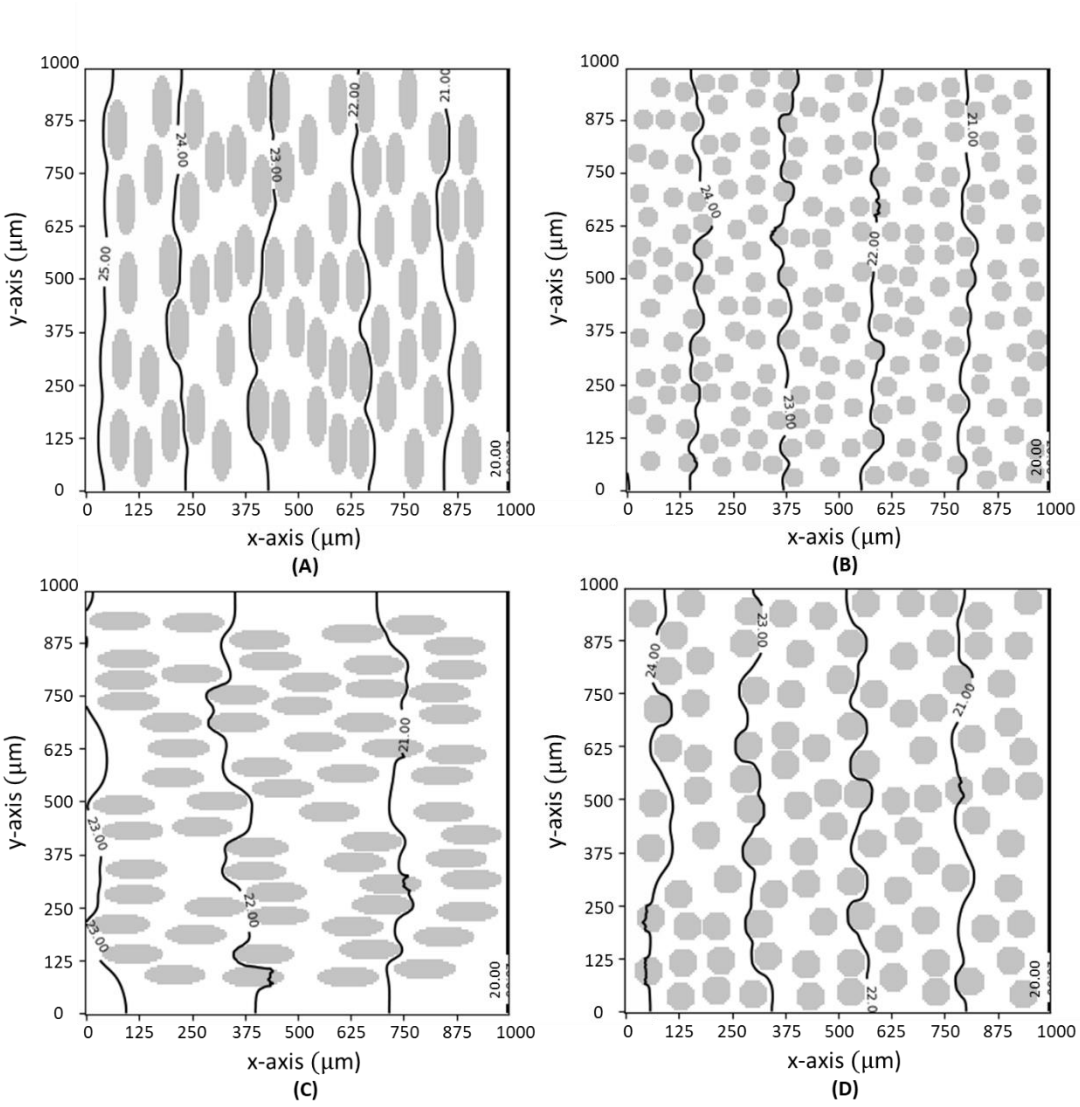

Citation:
Ke, X.; Duan, Y., A spatially-varying relaxation parameter Lattice Boltzmann Method (SVRP-LBM) for predicting the effective thermal conductivity of composite material. 2019, 169, 109080.
https://doi.org/10.1016/j.commatsci.2019.109080

Figure 13 Temperature contour plots at the equilibrium final state of simulated composite material reinforced by (A) elliptical fillers vertical to the heat flux direction, (B) spherical fillers with diameter of 50 μm, (C) elliptical fillers parallel to the heat flux direction, and (D) spherical fillers with diameter of 70 μm. The total filler volume fractions in all simulated materials were the same, 26.3±0.4%.

The ETCs of simulated composite materials are plotted as a function of filler volume fraction (φ) in Figure 14. The ETC values are calculated according to equation (14). The results show that the predicted ETC values always increase as the simulated filler volume fraction increase, same as what normally been observed from polymer composite reinforced by conductive fillers [6, 7, 50]. At the same filler volume fraction, the shape of the filler and its orientation show the dominate effect on the ETC, seeing Figure 14A. For materials reinforced by elliptical fillers with a long axis perpendicular to the heat flux direction, the predicted ETCs are much higher than that reinforced by spherical fillers. The lowest ETC is predicted as the composite is enforced by the elliptical filler with the long axis parallel to the heat flux direction. The differences between predicted ETC values between using elliptical fillers and spherical fillers increase as the filler volume fraction increases. The higher ETC of the composite containing elliptical fillers parallel to the heat flux direction is likely due to the enhanced thermal conductive path along the heat flux direction [16]. When the elliptical fillers are perpendicular to the heat flux, the thermal conductive path is enhanced along the y-axis (the major axis of the filler), however, the ETC is measured along the heat flux direction (x-direction). Since the minor axis of the elliptical filler is set to equal to the diameter of the spherical fillers, therefore at the same filler volume fraction, the filler volume density along the heat flux direction is higher in spherical filler geometry (Figure 13B) than that in the vertical elliptical fillers (Figure 13A). This might explain the lower ETC in the vertical elliptical fillers geometries than that in the dispersed spherical filler geometry.

Figure 14B compares the effect of filler scale on the ETC. The sphere filler is adopted in this study. The results show that simulated composite materials with larger particle sizes have higher ETC as predicted by LBM. This result is in good agreement with experimental observations [6, 50]. The similar trend was also reported by Zhou et al. [22] and Li et al. [7] using LBM methods, although different interfacial treatments between the filler and the composite matrix are applied in our study. As discussed previously, the efficiency of heat transfer within the sample domain would be slowed down when the heat flux goes from the highly conductive filler to the low conductivity matrix. Comparing with large filler particles, the small particles have higher specific surface area. Therefore, at the same total filler volume fraction, the number of lattice nodes experiencing this “slow down” process would be higher in simulated composite with smaller filler sizes.

Citation:
Ke, X.; Duan, Y., A spatially-varying relaxation parameter Lattice Boltzmann Method (SVRP-LBM) for predicting the effective thermal conductivity of composite material. 2019, 169, 109080.
https://doi.org/10.1016/j.commatsci.2019.109080

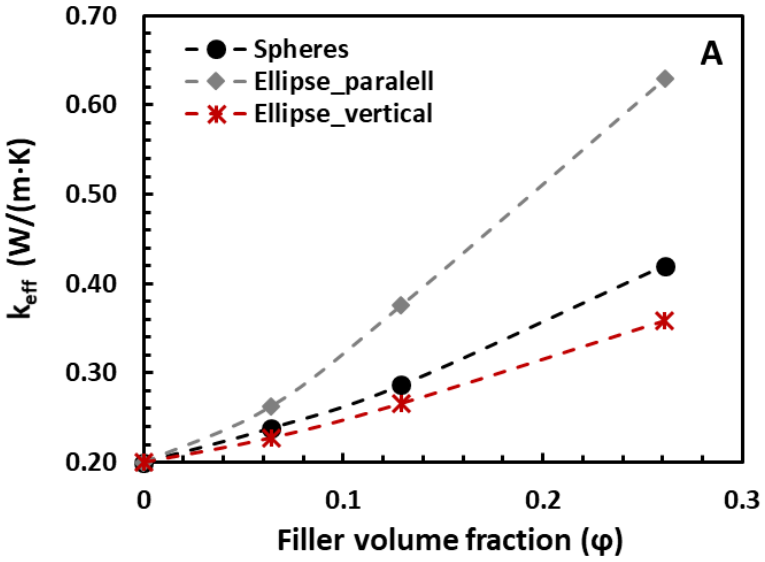

503

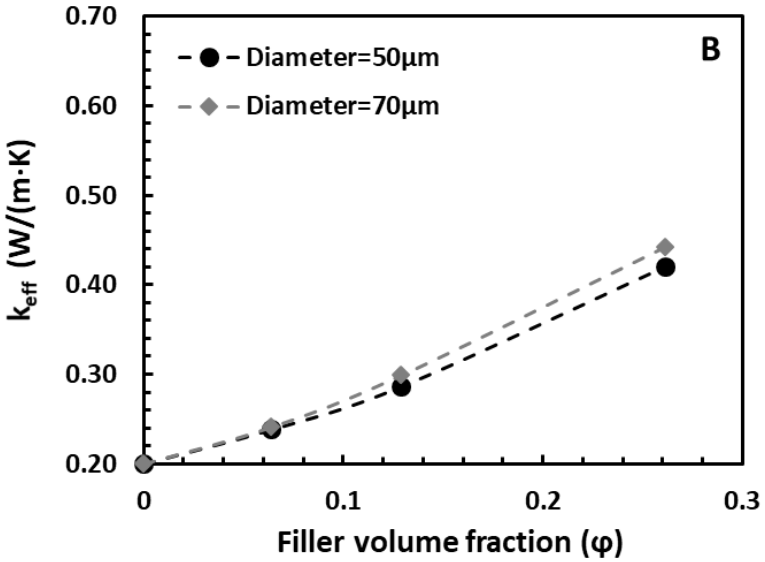

504

505 Figure 14 Comparison of effects of A) particle shapes and orientations, B) particle
506 sizes on the predicted effective thermal conductivities using LBM at different filler
507 volume fractions, where k_1/k_2=0.01, k_1=0.2 W/m·K.

508

509 Although the (diameter) size of the functional fillers is in positive correlation with
510 the thermal conduction efficiency in composite materials containing uni-sized fillers,
511 as suggested in Figure 14B and also supported by experimental observations [6, 50],
512 this positive correlation is nonlinear and controlled by varies factors [51]. One of
513 them is the varying filler size. Figure 15 compares the temperature contours in three
514 composite materials reinforced by spherical fillers with varying sizes. It should be
515 noted that the total filler volume fraction is fixed as 26.3±0.8%. The distribution of
516 the filler size follows the normal distribution, as defined in equation (17). In these
517 three cases, the average filler diameters are the same (50 μm), but the standard
518 deviations are 10.7 μm, 19.5 μm and 28.3 μm, respectively. Figure 15E shows the

fitted filler size distribution curve. Similar to that shown in Figure 13, the temperature field is influenced by the local microstructures, where much significant heterogeneous temperature distribution can be observed from the materials containing fillers of larger variance. Figure 15D summaries the predicted ETC of these three microstructures in comparison with fillers of uniform diameters (50μm). Although the average diameters are the same, the filler size variations result in enhancement of ETC of the matrix. As suggested by Li et al. [7], the filler size effect is particularly significant on ETC at higher filler volume fraction (>20%). This is because the composite containing fillers of larger size variation might be able to achieve more efficient filler packing, thus enhancing the thermal conduction path and improving the thermal conductivity. This matches with experimental observations where hybrid fillers can often achieve better enhanced ETC due to the enhanced thermal conduction path through the sample [50, 52].

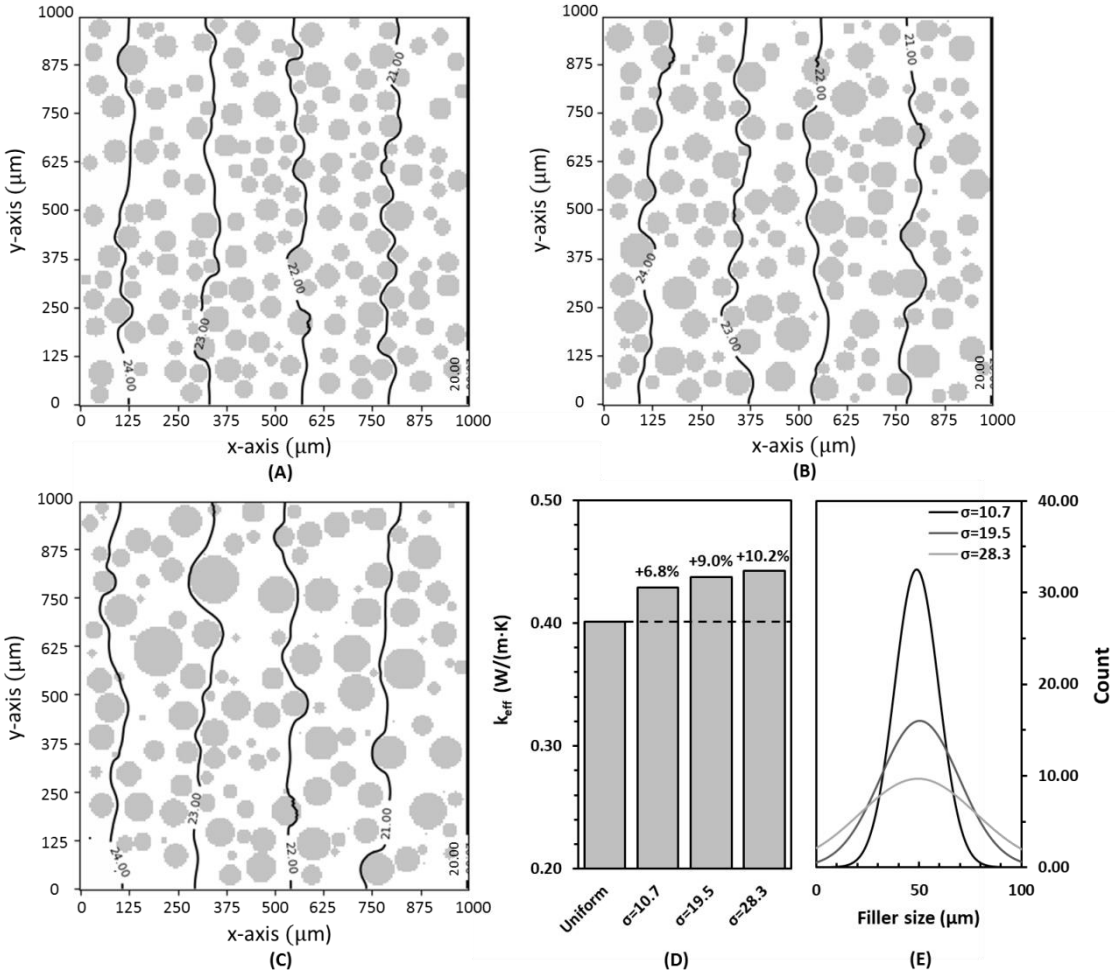

Figure 15 Temperature contour plots at the equilibrium final state of simulated composite material reinforced by spherical fillers of the different size distribution, (A) σ=10.7, (B) σ=19.5, (C) σ=28.3. For all these three simulated materials, the mean filler diameter is 50 μm and the total filler volume fractions are 26.3±0.8%. (D) The predicted ETC values and (E) the fitted filler size distribution curves, for each simulated microstructure.

Citation:
Ke, X.; Duan, Y., A spatially-varying relaxation parameter Lattice Boltzmann Method (SVRP-LBM) for predicting the effective thermal conductivity of composite material. 2019, 169, 109080.
https://doi.org/10.1016/j.commatsci.2019.109080

539

540 4.2 Thermal conduction between the filler and matrix interfaces

541 In this section, the thermal conduction between the filler and matrix interfaces in
542 composite material with/without the presence of contact resistance is studied. When
543 simulating the effect of contact resistance in composite materials, it is often practical
544 to use one or two lattices to represent the interfacial region [7], without having to
545 reflect the actual geometry of the rough interfaces. This suggests that instead of using
546 the thermal conductivity of air at the interfacial region, the ETC at the near interfacial
547 region (matrix-gap-filler) should be used. Since the interfacial contact resistance is
548 affected by various properties of the materials used, such as surface roughness,
549 particle sizes and geometries [53], the ETC value of the interfacial region can be
550 estimated either by either using theoretical ETC models [22, 45] or fitting of
551 experimental data [7].

552 However in this study, for the purpose of demonstrating the capability of this
553 SVRP-LBM solver to reflect the interfacial contact resistance, a simplified 2-D
554 geometry shown in Figure 16 is used, and the interfacial region is considered to be
555 filled with dry air. Three different types of interfacial treatments are studied, the
556 geometry CR=0 represents the perfect contact between filler and matrix interfaces,
557 while geometry CR=1 and CR=2 represent the scenarios of different contact
558 resistances due to the imperfect contact between the filler and matrix interfaces. The
559 comparison of temperature profiles at steady states between these three geometries
560 will be able to demonstrate the ability of this SVRP-LBM code to take into account
561 the effect of interfacial contact resistance where applicable.

562

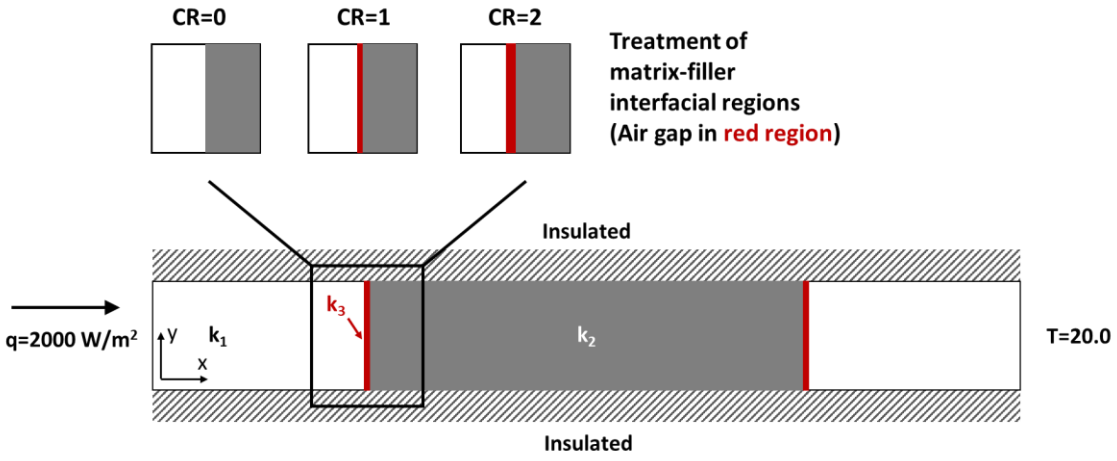

563

564 Figure 16 Schematic diagram of a 2-D geometry for study the effects of interfacial
565 contact resistance at the matrix-filler interfaces. Three different interfacial geometries
566 are used, replacing 0 (CR=0), 1 (CR=1) and 2 (CR=2) lattices at the matrix-filler
567 interfaces with air, where k_1=0.2 W/m·K (thermal conductivity of artificial matrix),
568 k_2=20 W/m·K (thermal conductivity of artificial filler) and k_3=0.026 W/m·K (thermal

Citation:
Ke, X.; Duan, Y., A spatially-varying relaxation parameter Lattice Boltzmann Method (SVRP-LBM) for predicting the effective thermal conductivity of composite material. 2019, 169, 109080.
https://doi.org/10.1016/j.commatsci.2019.109080

conductivity of dry air at 25 °C). The LBM lattice number of 404x50 is used for CR=0 and CR=2, while lattice number of 402x50 is used for CR=1.

The predicted ETC values of geometry CR=0, CR=1 and CR=2 are 0.39 W/m·K, 0.36 W/m·K, 0.34 W/m·K respectively, consistent with experimental observations where higher contact resistance resulted in lower thermal conductivities [36, 53, 54]. Figure 17 shows the temperature profiles of these three geometries at steady state along the heat flux direction. Among these three geometries, the temperature gradients within the same material (matrix or filler) are the same at steady state, following the Fourier's law for heat conduction. However, across the entire lattice domain, the temperature differences between the heat source and the isothermal side are higher in geometry CR=1 and CR=2 than CR=0. This is primarily due to the significant temperature drop in the air-filled region. Figure 17B-1 and Figure 17B-2 show more detailed comparison of the multi-phases regions between the filler-matrix interfaces. The simulation results show a larger temperature drop in geometry CR=2 than geometry CR=1 due to the wider air gap, reflecting a higher contact resistance.

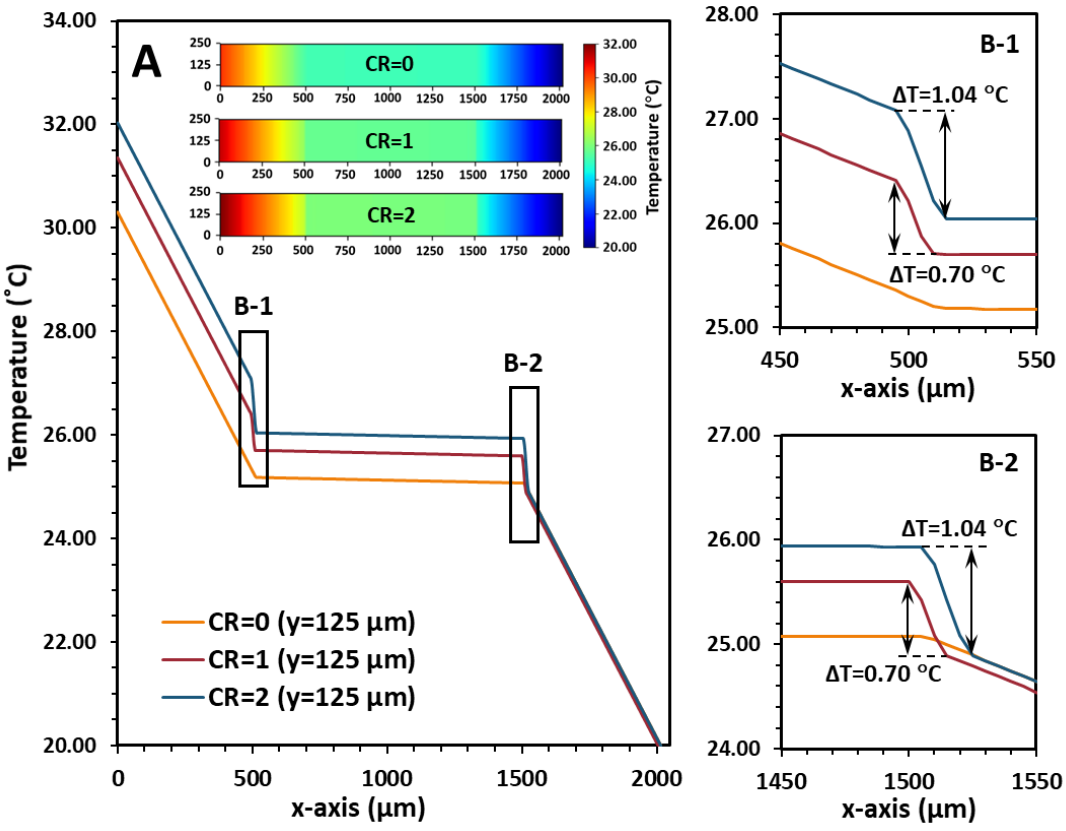

Figure 17 Temperature profiles of geometry CR=0, CR=1 and CR=2 at steady state along the heat flux direction. (A) Horizontally cross the entire geometry; and selected regions (B-1) from 150 µm to 550 µm; (B-2) from 1450 µm to 1550 µm.

Citation:
Ke, X.; Duan, Y., A spatially-varying relaxation parameter Lattice Boltzmann Method (SVRP-LBM) for predicting the effective thermal conductivity of composite material. 2019, 169, 109080.
https://doi.org/10.1016/j.commatsci.2019.109080

For the experimentally prepared composite materials, a larger air gap in between the matrix-filler interfaces can be caused by higher surface roughness. The absolute temperature drop at the matrix-to-filler (Figure 17B-1) and the filler-to-matrix (Figure 17B-2) interfaces are the same. This is because the three geometries described in Figure 16 are isotropic in the y-axis direction. At the interfacial region, the heat flux flow along the x-axis direction from the matrix-to-filler and from filler-to-matrix are the same. However, in the case of actual composite materials, the geometries can be much more complex with non-isotropic local microstructures. The heat flux entering and leaving the filler particle might not be the same, leading to different temperature differences [33]. The results shown in Figure 17 prove that this SVRP-LBM solver has the ability to reflect the effect of interfacial contact resistance in composite materials, although geometry configurations need to be considered according to different materials.

4.3 ETCs of real composite material

Before further discussion, we would like to highlight here that the experimental data used in this section for case studies were measured using the guarded hot plate method according to ASTM D5470-17 [55]. This method measures the ETC via monitoring the temperature changes through a thin layer of the composite materials, which is suitable to be simulated via a 2D geometry [22]. The accuracy of this experimental method is about $\pm 2\%$ when the thermal conductivity of the measured material is above 0.1 W/mK [47].

Figure 18 compares the measured ETC [25] and LBM predictions of solder composite reinforced by copper spheres at different filler volume fractions. The thermal physical properties of the matrix and the fillers are listed in Table 1. The random composite microstructure is again simulated using the RDFG method. The average filler diameter matches with the actual experimental value (500 μm). No filler size variation is applied according to [25]. Different numbers of fillers are included in the lattice domain in order to simulate filler volume fractions varying from 0.016 to 0.296. As shown in Figure 18, the LBM predicted ETC agrees well with the measurements, as well as the theoretical predictions using the Maxwell-Eucken model. It suggests that the LBM algorithm developed in this study can accurately predict the ETC of real composite material reinforced by well-dispersed sphere fillers.

Citation:
Ke, X.; Duan, Y., A spatially-varying relaxation parameter Lattice Boltzmann Method (SVRP-LBM) for predicting the effective thermal conductivity of composite material. 2019, 169, 109080.
https://doi.org/10.1016/j.commatsci.2019.109080

Table 1 Thermophysical properties of materials chosen for case studies.

	Thermal diffusivity coefficient D (m^2/s)	Thermal conductivity K (W/(m·K)	Density ρ· (kg/m^3)	Specific thermal capacity Cp (J/(kg·K)	Ref
Copper	116.00×10^{-6}	398.00	8940	384	[25]
Solder	34.80×10^{-6}	78.10	7360	305	[25]
Silicon rubber	0.10×10^{-6}	0.15	980	1590	[6]
Al_2O_3	8.74×10^{-6}	30.00	3900	880	[6]

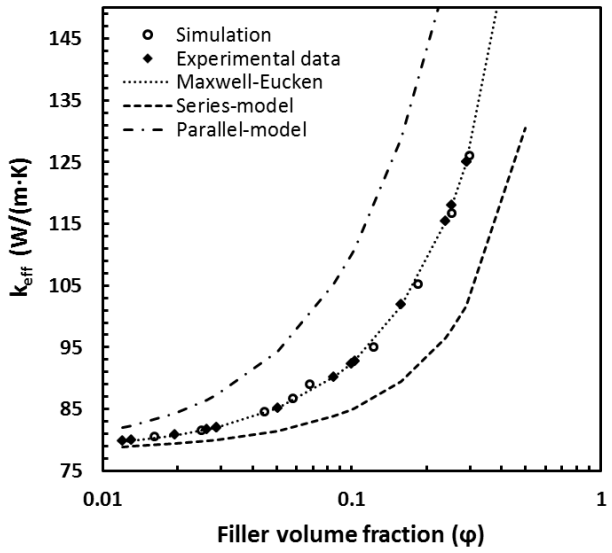

Figure 18 Comparison between experimental data and LBM predicted values of solder composite reinforced with copper spheres [25].

Figure 19 shows the measured ETC of silicon rubber reinforced by Al_2O_3 fillers of four different particle sizes sourced from the experimental data shown in [6, 12], and the corresponded LBM results using either spherical or elliptical fillers. The calculation using different empirical models are presented in the figure. The thermal physical properties used for simulations can also be found in Table 1. The mean diameter sizes of both spherical and elliptical fillers are set as equal to the mean particle size reported in [6, 12] (d=75 μm, 35 μm, 10 μm or 3 μm). A relative standard deviation (σ/ξ) of 0.1 is applied to all LBM cases to reflect the filler size variation, as approximated from particle size distribution reported in the literature [6]. The aspect ratio of the elliptic filler is fixed as 3:1.

As illustrated in the Figure 19 (A-C), when the average filler sizes are larger than 10 μm and the filler volume fraction is higher than 0.1, both the Maxwell-Eucken model and the LBM model with spherical filler under-predict the ETC. Moreover, the

Citation:
Ke, X.; Duan, Y., A spatially-varying relaxation parameter Lattice Boltzmann Method (SVRP-LBM) for predicting the effective thermal conductivity of composite material. 2019, 169, 109080.
https://doi.org/10.1016/j.commatsci.2019.109080

predicted ETC using spherical fillers follows the Maxwell-Eucken prediction at lower filler volume fraction (<0.2), while at higher filler volume fraction, the LBM predictions using spherical fillers are slightly higher than the Maxwell-Eucken prediction. The same phenomenon has been observed from the mass diffusion process in porous media, where the LBM prediction is always higher than the Maxwell-Eucken model prediction in high porosity media [56]. The positive contribution of the particle size variation as discussed in section 4.1 may be one of the reasons.

When using ellipses fillers with an aspect ratio of 3:1, positioned parallel to the heat flux direction, the predicted ETC using the elliptical fillers showed good agreement with the experimental results when the average filler sizes are above 10 μm. The scanning electron microscope (SEM) images of the Al_2O_3 filler particles used for preparing this composite material showed plate-shaped geometry [12, 57]. The shape-effect of the filler, as discussed in the previous section, might explain the good performance of the LBM model with ellipses filler, which might also explain the under-prediction of the Maxwell-Eucken model and the LBM model with spherical filler.

Additionally, Xu et al [58] proposed a reconstructed Maxwell-Eucken model to fit the experimental data, contributing the higher ETC to the contact resistance between the particles. The reconstructed model fitted to these experimental data has also been plotted in Figure 19. In comparison with the reconstructed Maxwell-Eucken model, the LBM prediction using elliptical fillers also shows better agreement with experimental data (for filler size above 10 μm). The reconstructed model proposed by Xu et al. [58] is based on the assumption that every two particles will be connected together (with additional contact resistance between the two particles), which shares some similarities with the elliptical fillers.

In the cases of the smallest filler (ξ=3 μm Figure 19D), the LBM model with elliptical fillers leads to over-prediction of ETC; while the use of spherical fillers results in closer predictions. For commonly used non-spherical filler particles, such as Al_2O_3, ZnO, TiB_2, SiC and talc, the same material with very small particle sizes often possess the sphere-like feature [12, 43, 57], while larger particles often possess the non-spherical feature This is similar to that has been observed from carbon nanotube (CNT) reinforced composite, where larger CNT showed higher aspect ratio and led to higher ETC [59, 60]. This further supports the assumptions that the geometry effect could be one of the main factors that led to the greater enhanced ETCs of larger Al_2O_3 particles reinforced composite materials at high filler volume fraction.

Citation:
Ke, X.; Duan, Y., A spatially-varying relaxation parameter Lattice Boltzmann Method (SVRP-LBM) for predicting the effective thermal conductivity of composite material. 2019, 169, 109080.
https://doi.org/10.1016/j.commatsci.2019.109080

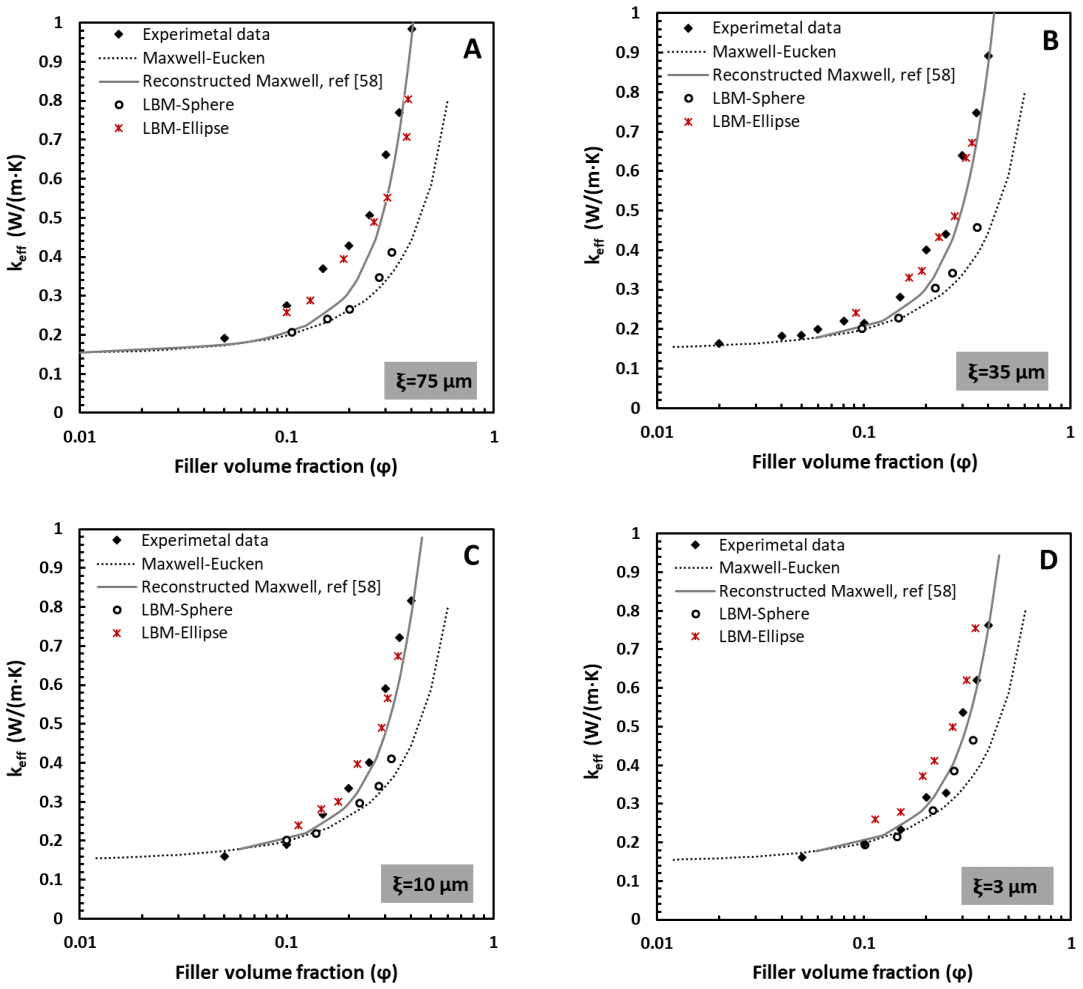

Figure 19 Experimental data, LBM prediction and empirical model output of ETCs of silicon rubber reinforced with Al_2O_3 fillers [6, 12].

5 Conclusion

The in-house coded spatially-varying relaxation parameter Lattice Boltzmann Method (SVRP-LBM) solver has been validated for predicting the effective thermal conductivity (ETC) of various composite materials, including simulating the interfacial contact resistance. It is found that higher prediction accuracy can be achieved when the lowest chosen relaxation parameter approaches 1.0, for composite materials with large thermal diffusivity ratios. The predictions also showed good agreement with experiments data when choosing the right representative filler geometries.

The effects of filler geometry (orientation and shape) and filler size variation on the thermal conduction behaviour of simulated composite material are assessed using SVRP-LBM solver. The predicted ETC increases as the filler volume fraction

increases. At the same filler volume fraction, the elliptical fillers parallel to the heat flow direction achieved the highest ETC, possibly attributed by the enhanced thermal conduction path along the heat flux direction. Higher filler size variance can result in higher ETC, likely due to the improved filler packing efficiency.

The SVRP-LBM solver developed in this study can be used to design filler reinforced composite material with targeted ETC and local temperature distribution requirement. As the initial development of a predictive design tool for functional composite materials, an extension of this method to the three-dimensional solver and quantification of uncertainties brought by the random location effect will further improve the accuracy of this model, which will be discussed in future studies.

Acknowledgement

The participation of XK was sponsored by University of Bath Prize Fellowship.

Data Availability

The raw and processed data required to reproduce these findings cannot be shared at this time as the data also forms part of an ongoing study.

References

1. Mamunya, Y.P., et al., *Electrical and thermal conductivity of polymers filled with metal powders.* European Polymer Journal, 2002. **38**(9): p. 1887-1897.
2. Fu, Y.-X., et al., *Thermal conductivity enhancement of epoxy adhesive using graphene sheets as additives.* International Journal of Thermal Sciences, 2014. **86**: p. 276-283.
3. Tong, X.C., *Advanced Materials for Thermal Management of Electronic Packaging*. Vol. 30. 2011: Springer-Verlag New York. 618.
4. Agyenim, F., et al., *A review of materials, heat transfer and phase change problem formulation for latent heat thermal energy storage systems (LHTESS).* Renewable and Sustainable Energy Reviews, 2010. **14**(2): p. 615-628.
5. Mukherjee, P.P., Q. Kang, and C.-Y. Wang, *Pore-scale modeling of two-phase transport in polymer electrolyte fuel cells—progress and perspective.* Energy & Environmental Science, 2011. **4**(2): p. 346-369.
6. Gao, B.Z., et al., *Experimental and theoretical studies of effective thermal conductivity of composites made of silicone rubber and Al2O3 particles.* Thermochimica Acta, 2015. **614**: p. 1-8.
7. Li, L., et al., *Study on effective thermal conductivity of silicone/phosphor composite and its size effect by Lattice Boltzmann method.* Heat and Mass Transfer, 2016. **52**(12): p. 2813-2821.
8. Sengul, O., et al., *Effect of expanded perlite on the mechanical properties and thermal conductivity of lightweight concrete.* Energy and Buildings, 2011. **43**(2): p. 671-676.

9. Cahill, D.G., et al., *Nanoscale thermal transport.* Journal of Applied Physics, 2003. **93**(2): p. 793-818.
10. Burger, N., et al., *Review of thermal conductivity in composites: Mechanisms, parameters and theory.* Progress in Polymer Science, 2016. **61**: p. 1-28.
11. Hussain, A.R.J., et al., *Review of polymers for heat exchanger applications: Factors concerning thermal conductivity.* Applied Thermal Engineering, 2017. **113**: p. 1118-1127.
12. Sim, L.C., et al., *Thermal characterization of Al2O3 and ZnO reinforced silicone rubber as thermal pads for heat dissipation purposes.* Thermochimica Acta, 2005. **430**(1): p. 155-165.
13. Fu, Y.-X., et al., *Thermal conductivity enhancement with different fillers for epoxy resin adhesives.* Applied Thermal Engineering, 2014. **66**(1): p. 493-498.
14. Zhai, S., et al., *Effective thermal conductivity of polymer composites: Theoretical models and simulation models.* International Journal of Heat and Mass Transfer, 2018. **117**: p. 358-374.
15. Tekce, H.S., D. Kumlutas, and I.H. Tavman, *Effect of Particle Shape on Thermal Conductivity of Copper Reinforced Polymer Composites.* Journal of Reinforced Plastics and Composites, 2007. **26**(1): p. 113-121.
16. Chen, H., et al., *Thermal conductivity of polymer-based composites: Fundamentals and applications.* Progress in Polymer Science, 2016. **59**: p. 41-85.
17. Benveniste, Y., *Effective thermal conductivity of composites with a thermal contact resistance between the constituents: Nondilute case.* Journal of Applied Physics, 1987. **61**(8): p. 2840-2843.
18. Mori, T. and K. Tanaka, *Average stress in matrix and average elastic energy of materials with misfitting inclusions.* Acta Metallurgica, 1973. **21**(5): p. 571-574.
19. Azadi, P., R. Farnood, and N. Yan, *FEM–DEM modeling of thermal conductivity of porous pigmented coatings.* Computational Materials Science, 2010. **49**(2): p. 392-399.
20. Duan, Y., et al., *Analysis of the horizontal flow in the advanced gas-cooled reactor.* Nuclear Engineering and Design, 2014. **272**: p. 53-64.
21. Wang, M., et al., *Mesoscopic predictions of the effective thermal conductivity for microscale random porous media.* Physical Review E, 2007. **75**(3): p. 036702.
22. Zhou, F. and G. Cheng, *Lattice Boltzmann model for predicting effective thermal conductivity of composite with randomly distributed particles: Considering effect of interactions between particles and matrix.* Computational Materials Science, 2014. **92**: p. 157-165.
23. Walther, E., R. Bennacer, and C. De Sa, *Lattice Boltzmann Method and diffusion in materials with large diffusivity ratios.* Thermal science, 2017. **21**(3): p. 1173–1182.
24. Cao, A. and J. Qu, *Size dependent thermal conductivity of single-walled carbon nanotubes.* Journal of Applied Physics, 2012. **112**(1): p. 013503.
25. Lee, H.J. and R.E. Taylor, *Thermal diffusivity of dispersed composites.* Journal of Applied Physics, 1976. **47**(1): p. 148-151.
26. Sanada, K., Y. Tada, and Y. Shindo, *Thermal conductivity of polymer composites with close-packed structure of nano and micro fillers.* Composites Part A: Applied Science and Manufacturing, 2009. **40**(6): p. 724-730.

27. Wang, M. and N. Pan, *Modeling and prediction of the effective thermal conductivity of random open-cell porous foams.* International Journal of Heat and Mass Transfer, 2008. **51**(5): p. 1325-1331.
28. Lu, J.H., H.Y. Lei, and C.S. Dai, *A lattice Boltzmann algorithm for simulating conjugate heat transfer through virtual heat capacity correction.* International Journal of Thermal Sciences, 2017. **116**: p. 22-31.
29. Fang, W.-Z., et al., *Predictions of effective thermal conductivities for three-dimensional four-directional braided composites using the lattice Boltzmann method.* International Journal of Heat and Mass Transfer, 2016. **92**: p. 120-130.
30. Krüger, T., et al., *The Lattice Boltzmann Method: Principles and Practice*. 2016: Springer International Publishing.
31. Wang, J., M. Wang, and Z. Li, *A lattice Boltzmann algorithm for fluid–solid conjugate heat transfer.* International Journal of Thermal Sciences, 2007. **46**(3): p. 228-234.
32. Evans, W., et al., *Effect of aggregation and interfacial thermal resistance on thermal conductivity of nanocomposites and colloidal nanofluids.* International Journal of Heat and Mass Transfer, 2008. **51**(5-6): p. 1431-1438.
33. Deng, Z., et al., *Heat Conduction in Porous Media Characterized by Fractal Geometry.* Energies, 2017. **10**(8): p. 1230.
34. Pollack, G.L., *Kapitza Resistance.* Reviews of Modern Physics, 1969. **41**(1): p. 48-81.
35. Nan, C.-W., et al., *Interface effect on thermal conductivity of carbon nanotube composites.* Applied Physics Letters, 2004. **85**(16): p. 3549-3551.
36. Gharagozloo-Hubmann, K., et al., *Filler geometry and interface resistance of carbon nanofibres: Key parameters in thermally conductive polymer composites.* Applied Physics Letters, 2013. **102**(21): p. 213103.
37. Wang, Z.L., et al., *Thermal boundary resistance and temperature dependent phonon conduction in CNT array multilayer structure.* International Journal of Thermal Sciences, 2013. **74**: p. 53-62.
38. Mohamad, A., *Lattice Boltzmann Method Fundamentals and Engineering Applications with Computer Codes*. 2011.
39. Bhatnagar, P.L., E.P. Gross, and M. Krook, *A Model for Collision Processes in Gases. I. Small Amplitude Processes in Charged and Neutral One-Component Systems.* Physical Review, 1954. **94**(3): p. 511-525.
40. Zou, Q. and X. He, *On pressure and velocity boundary conditions for the lattice Boltzmann BGK model.* Physics of Fluids, 1997. **9**(6): p. 1591-1598.
41. Zain-ul-abdein, M., et al., *Numerical investigation of the effect of interfacial thermal resistance upon the thermal conductivity of copper/diamond composites.* Materials & Design, 2015. **86**: p. 248-258.
42. Kim, C.P., et al., *Processing of carbon-fiber-reinforced Zr41.2Ti13.8Cu12.5Ni10.0Be22.5 bulk metallic glass composites.* Applied Physics Letters, 2001. **79**(10): p. 1456-1458.
43. Guise, O., C. Strom, and N. Preschilla, *STEM-in-SEM method for morphology analysis of polymer systems.* Polymer, 2011. **52**(5): p. 1278-1285.
44. Shakoor, A. and N.L. Thomas, *Talc as a nucleating agent and reinforcing filler in poly(lactic acid) composites.* Polymer Engineering & Science, 2014. **54**(1): p. 64-70.
45. Mohamad, A.A., et al., *Treatment of Transport at the Interface Between Multilayers via the Lattice Boltzmann Method.* Numerical Heat Transfer, Part B: Fundamentals, 2015. **67**(2): p. 124-134.

46. Maxwell, J.C., *A treatise on electricity and magnetism*. 1881: Clarendon Press.
47. Hammerschmidt, U., *Guarded Hot-Plate (GHP) Method: Uncertainty Assessment.* International Journal of Thermophysics, 2002. **23**(6): p. 1551-1570.
48. Deissler, R.G. and J.S. Boegli, *An investigation of effective thermal conductivities of powders in various gases.* Trans. Am. Soc. Mech. Engrs., 1958: p. Medium: X; Size: Pages: 1417-25.
49. Xu, Y. and K. Yagi, *Automatic FEM model generation for evaluating thermal conductivity of composite with random materials arrangement.* Computational Materials Science, 2004. **30**(3): p. 242-250.
50. Mu, Q., S. Feng, and G. Diao, *Thermal conductivity of silicone rubber filled with ZnO.* Polymer Composites, 2007. **28**(2): p. 125-130.
51. Nan, C.-W., et al., *Effective thermal conductivity of particulate composites with interfacial thermal resistance.* Journal of Applied Physics, 1997. **81**(10): p. 6692-6699.
52. Choi, S. and J. Kim, *Thermal conductivity of epoxy composites with a binary-particle system of aluminum oxide and aluminum nitride fillers.* Composites Part B: Engineering, 2013. **51**: p. 140-147.
53. Zhang, P., Q. Li, and Y. Xuan, *Thermal contact resistance of epoxy composites incorporated with nano-copper particles and the multi-walled carbon nanotubes.* Composites Part A: Applied Science and Manufacturing, 2014. **57**: p. 1-7.
54. Sadeghi, E., S. Hsieh, and M. Bahrami, *Thermal conductivity and contact resistance of metal foams.* Journal of Physics D: Applied Physics, 2011. **44**(12): p. 125406.
55. ASTM, *D5470-17*, in *Standard Test Method for Thermal Transmission Properties of Thermally Conductive Electrical Insulation Materials*. 2017, ASTM International: West Conshohocken, PA.
56. Xuan, Y.M., K. Zhao, and Q. Li, *Investigation on mass diffusion process in porous media based on Lattice Boltzmann method.* Heat and Mass Transfer, 2010. **46**(10): p. 1039-1051.
57. Hill, R.F. and P.H. Supancic, *Thermal Conductivity of Platelet-Filled Polymer Composites.* Journal of the American Ceramic Society, 2002. **85**(4): p. 851-857.
58. Xu, J.Z., B.Z. Gao, and F.Y. Kang, *A reconstruction of Maxwell model for effective thermal conductivity of composite materials.* Applied Thermal Engineering, 2016. **102**: p. 972-979.
59. Deng, F., et al., *Effects of anisotropy, aspect ratio, and nonstraightness of carbon nanotubes on thermal conductivity of carbon nanotube composites.* Applied Physics Letters, 2007. **90**(2): p. 021914.
60. Li, J., et al., *Correlations between Percolation Threshold, Dispersion State, and Aspect Ratio of Carbon Nanotubes.* Advanced Functional Materials, 2007. **17**(16): p. 3207-3215.